Journal of Alloys and Compounds 509 (2011) 8742–8747

Contents lists available at ScienceDirect

Journal of Alloys and Compounds

journal homepage: www.elsevier.com/locate/jallcom

A new precipitation based method for preparation of metasilicate phosphors

G.J. Talwar[c,*], C.P. Joshi[a], S.V. Moharil[b], S.M. Dhopte[c], P.L. Muthal[c], V.K. Kondawar[c]

[a] Physics Department, Shri Ramdeobaba K.N. Engineering College, Katol Road, Nagpur 440013, India
[b] Department of Physics, Rashtrasant Tukdoji Maharaj Nagpur University, Nagpur, India
[c] National Environmental Engineering Research Institute, Nehru Marg, Nagpur, India

ARTICLE INFO

Article history:
Received 9 January 2011
Received in revised form 7 June 2011
Accepted 13 June 2011
Available online 17 June 2011

Keywords:
Photoluminescence
Ns2 activator
Silicate
Phosphor

ABSTRACT

Metasilicates are important class of materials. They find applications in many diverse areas. Silicates are widely used as adsorbents, sensors, in production of ceramics, as bioactive materials, as microwave dielectric etc. A large number of phosphors based on metasilicate hosts are known. The conventional routes for synthesis of silicates are the solid state reaction and sol–gel. The synthesis temperature for metasilicates is usually in excess of 1100 °C. Here, we report for the first time the wet-chemical preparation of alkaline earth metasilicates. Though the as-prepared compounds were poorly crystallized, annealing at 700 °C was sufficient for the formation of well defined crystalline phases. Photoluminescence was also observed in these compounds after activating with suitable dopants.

1. Introduction

Silicates are most abundant in nature. Depending upon Si:O ratio, they are classified as ortho (1:4), meta (1:3) and pyro (2:7) silicates [1]. A more detailed classification is made on the basis of criteria like coordination number of Si, number of (Si,O)-polyhedra, multiplicity, etc. [2]. They find applications in many diverse areas [3]. Silicates are widely used as adsorbents of polysaccharides [4] and numerous ions such as lead or calcium [5], as potentiometric sensors of hydrogen ions [6], in production of ceramics [7] or for sorption of atmospheric CO_2 [8], to recover cerium from radioactive waste materials and to adsorb Nd^{3+} ions [9], as bioactive materials [10,11], as microwave dielectric [12], etc. As a kind of biodegradable ceramic with good bioactivity, beta-$CaSiO_3$ has been widely used for preparation of beta-$CaSiO_3$/biopolymer composite scaffolds and has been proved to be an effective additive to create bioactive composites [13–15]. Stratified natural silicates are also used as carriers of plant protection agents [16].

$CaSiO_3$ exists in several polymorphs such as alpha-$CaSiO_3$ (pseudowollastonite), triclinic beta-CaSiO3 (wollastonite), monoclinic beta-$CaSiO_3$ (parawollastonite) and high-pressure $CaSiO_3$ [17]. Wollastonite ($CaSiO_3$) has received considerable attention due to its good bioactivity and biocompatibility in recent years [18–21]. Some investigators have pointed out that the bioactivity determined by the rate of hydroxyapatite formation on wollastonite ceramics in SBF solutions is higher than that of the other biocompatible glass and glass ceramics [22]. Traditionally, wollastonite powders were prepared by solid-state reaction at high calcination temperatures over 1100 °C [23], which induces sintering and aggregation of particles. Furthermore, the milling process to reduce the particle size generally yields non-homogeneous mixtures on a microscopic scale and induces lattice strains in the material [24]. α-$CaSiO_3$ is obtained by heating the beta form above 1150 °C. The actual transition temperature is susceptible to impurity contents [25]. The addition of ions smaller than calcium, such as magnesium, stabilizes the beta $CaSiO_3$ structure, whereas the addition of ions larger than calcium, such as strontium, stabilizes the alpha-$CaSiO_3$ structure.

$SrSiO_3$ exists as-alpha $SrSiO_3$ [space group C2/c (15)] and two high pressure phases designated as delta and delta′ [26]. A phase stable in the interval 34–59 kbar was originally assigned orthorhombic structure which was later corrected to monoclinic. In alpha $SrSiO_3$ [27] the Sr atoms occupy three kinds of sites [Sr(1), Sr(2) and Sr(3)], which are surrounded by eight O atoms with Sr–O distances of 2.39 (1)–2.83 (1) Å. Three of the distorted SiO_4 tetrahedra with Si–O bond lengths of 1.48 (1)–1.85 (2) Å form a (Si_3O_9) 6-ring by sharing O atoms. The structure consists of Sr^{2+} ions and (Si_3O_9) 6 rings alternately packed along the direction perpendicular to (0 0 1).

The compound $BaSiO_3$ crystallizes in two polymorphic varieties, with a ring structure (pseudowollastonite, $a = 7.50$ Å, $c = 10.58$ Å) (also known as hexagonal, alpha) and a chain structure (pyroxenoid, $a = 4.54$ Å, $b = 5.56$ Å, $c = 12.27$ Å) (also known as orthorhombic, beta) [28,29]. In solid phase synthesis, $BaSiO_3$ is crystallized in the chain polymorphic form.

* Corresponding author. Tel.: +91 712 2283708; fax: +91 712 2249875.
E-mail addresses: gurjeet_talwar05@yahoo.co.in (G.J. Talwar), svmoharil@yahoo.com (S.V. Moharil).

0925-8388/$ – see front matter © 2011 Elsevier B.V. All rights reserved.
doi:10.1016/j.jallcom.2011.06.043

A large number of phosphors based on metasilicate hosts are known. $CaSiO_3$ activated with Pb and Mn is one of the earliest known, red emitting phosphor [30]. More recent works report luminescence of doubly activated (Eu,Bi) $CaSiO_3$ [31] and $SrSiO_3$ [32]. Use of Eu^{2+}/Sm^{3+} doped $SrSiO_3$ for white light emitting diodes has been proposed by Cui et al. [33]. $MgSiO_3$:Eu^{2+}, Dy^{3+}, Mn^{2+} was discovered as a red emitting, long lasting phosphor [34]. The conventional routes for synthesis of silicates are the solid state reaction and sol–gel [35]. The former is used very widely [36,37]. The synthesis temperature for metasilicates is usually in excess of 1100 °C. There are not many attempts to prepare silicates by precipitation. Most of the silicates are insoluble in water and thus there are problems in choosing the water soluble precipitating agent. Na_2SiO_3 is one of the rare, water soluble silicate. However, even today, the nature of silicate molecules in the solution is far from clear, many contradictory data have been published regarding these issues [38]. In this paper we describe a new precipitation based synthesis of some alkaline earth metasilicates using Na_2SiO_3 as a precipitating agent.

2. Experimental

All ingredients used in the synthesis are of Analytical Reagent grade. Metasilicates were precipitated from aqueous solutions of metal nitrates by slowly adding Na_2SiO_3 solution. The precipitate formed was filtered, dried and then annealed in air at 700 °C for 1 h. For preparing various activated phosphors, appropriate metal nitrate was added in the desired quantity to the starting solution and similar procedure was followed. In some cases, for reducing the Cerium and tin activators to the desired trivalent/divalent state, the phosphors were heated at 700 °C in the reducing atmosphere provided by burning charcoal. X-ray diffraction patterns were recorded on Philips PANalytical X'pert Pro diffractometer. Cu line (1.54056 Å) was used. Measurements were made in steps of 0.02° over the range 10–80°. PL characteristics were studied using a Hitachi F-4000 spectrofluorimeter, at room temperature, using 1.5 nm spectral slit width in the range of 200–700 nm. Xenon lamp was used as a source of excitation.

3. Results and discussion

3.1. $CaSiO_3$

As precipitated powder was poorly crystallized and no sharp line pattern was observed. The samples annealed at 700 °C for 1 h showed good crystallinity. Fig. 1 shows stick patterns deduced from the diffraction data obtained for the annealed $CaSiO_3$ samples. The patterns are compared with the major lines in the ICDD data file 76-0186 corresponding to beta-$CaSiO_3$ which crystallizes in triclinic structure (space group P-1) with 6 formula units in the unit cell having lattice parameters $a = 7.94$, $b = 7.32$, $c = 7.07$, alpha 90°02′, beta 95°22′ and gamma 103°26′ (Fig. 2). An excellent match is seen. $CaSiO_3$ is thus formed at annealing temperature as low as 700 °C by the procedure described here.

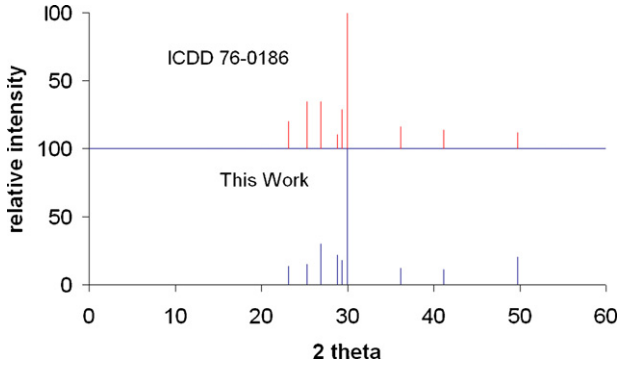

Fig. 1. XRD pattern for $CaSiO_3$. Stick pattern deduced from XRD data recorded for $CaSiO_3$ are compared with the major lines in the ICDD data file 76-0186. An excellent match is seen.

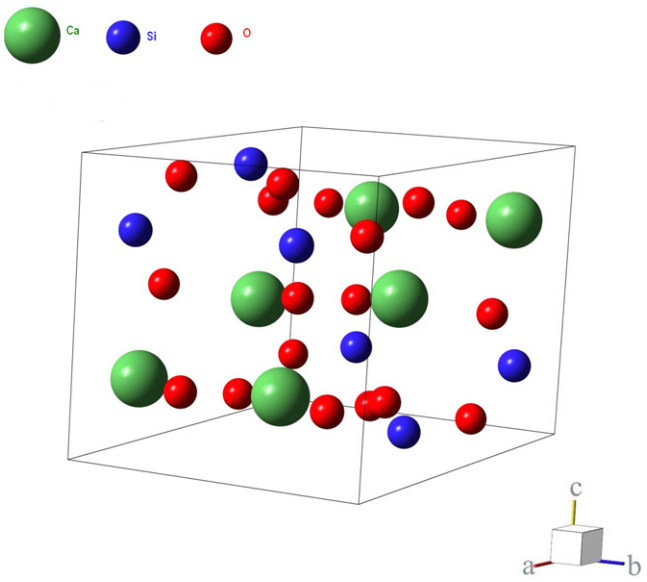

Fig. 2. Unit cell of beta $CaSiO_3$.

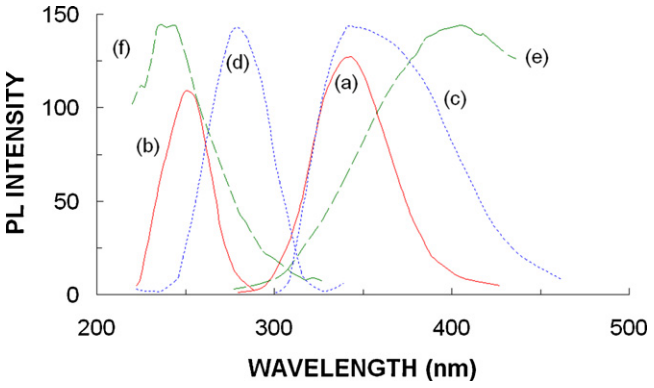

Fig. 3. Photoluminescence (PL) spectra of ns^2 activators in $CaSiO_3$. (a) Pb^{2+} emission for 256 nm excitation; (b) Pb^{2+} excitation for 340 nm emission; (c) Bi^{3+} emission for 284 nm excitation; (d) Bi^{3+} excitation for 347 nm emission; (e) Sn^{2+} emission for 237 nm excitation; (f) Sn^{2+} excitation for 413 nm emission.

Fig. 3 shows PL results for some ns^2 activators. For ns^2 type impurities, the ground level is $^1S_0$ arising from the s^2 configuration and the lowest excited levels are $^3P_0$, $^3P_1$ and $^1P_1$ derived from the excited sp configuration. The absorption spectra of ns^2 ions in solids consist of three main bands labeled A, B and C in order of increasing energy corresponding to transitions $^1S_0 \rightarrow {}^3P_0$, $^3P_1$ and $^1P_1$, respectively. The C band corresponds to allowed transition, whereas transitions corresponding to A and B bands are only partly allowed by spin-orbit coupling and vibronic coupling, respectively. The A band lies in the UV range. It is markedly sensitive to the environment [39,40]. The lower-lying $^3P_0$ and $^3P_1$ excited state levels are responsible for the luminescence features. The transition from $^3P_0$ to the ground $^1S_0$ state is J–J forbidden and only weakly allowed by phonon interactions. It is thus characterized by long radiative lifetime; of the order of milliseconds. The transition from $^3P_1$ to $^1S_0$ ground state is partly allowed due to the spin–orbit coupling which mixes the spin-allowed $^1P_1$ level with $^3P_1$ level. Such a mixing results in the radiative lifetime of the order of hundreds of nanoseconds [41]. The $^3P_0$ level is usually called metastable, while the $^3P_1$ level is often referred to as radiative. $^3P_1$ and $^3P_0$ levels are close enough to obtain the thermal population of the $^3P_1$ level from $^3P_0$ at higher temperatures.

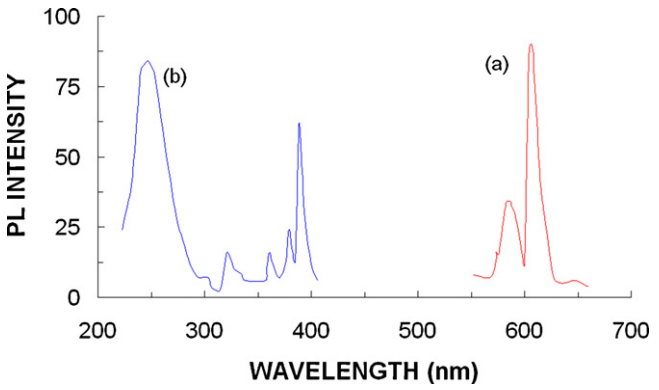

Fig. 4. Photoluminescence (PL) spectra of $CaSiO_3$:Eu^{3+}. (a) Eu^{3+} emission for 254 nm excitation; (b) Eu^{3+} excitation for 613 nm emission.

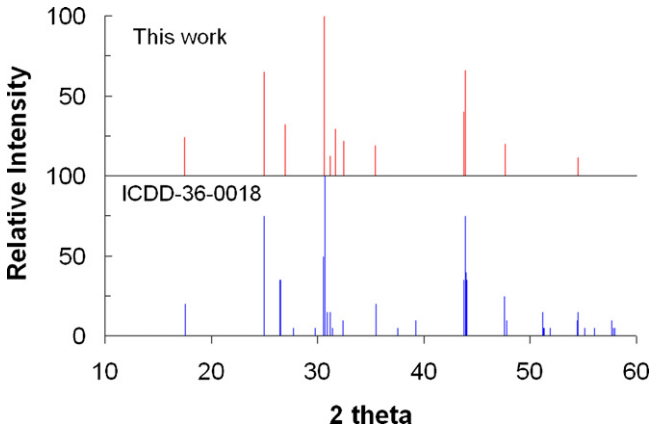

Fig. 5. XRD pattern for $SrSiO_3$. Stick pattern deduced from XRD data recorded for $SrSiO_3$ are compared with the major lines in the ICDD data file 36-0018 corresponding to monoclinic alpha-$SrSiO_3$. An excellent match is seen.

Pb^{2+} emission is in UV region around 340 nm (Fig. 3, curve a). The corresponding excitation maximum is at 256 nm (Fig. 3, curve b). These results are in excellent agreement with those reported by Frolich [30]. $CaSiO_3$:Pb and related phosphors have been studied quite early. The old work is reviewed by Klasens et al. [42].

UV emission is also observed in $CaSiO_3$ activated by Bi^{3+}. The position of the emission maximum (347 nm) is quite close to that observed for Pb^{2+} (Fig. 3, curve c). However, the excitation maximum is observed at longer wavelengths (Fig. 3, curve d) around 284 nm. We did not find any literature on Bi^{3+} emission in triclinic $CaSiO_3$. Excitation spectrum for Bi^{3+} in monoclinic $CaSiO_3$ contains a band at 359 nm corresponding to $^1S_0 \rightarrow {}^3P_1$ transition [31].

Very weak emission was observed for Sn^{2+} activation. The violet emission peaks around 410 nm when excited by 237 nm (Fig. 3, curves e and f). On the other hand, Mooney [25] observed strong green emission in beta $CaSiO_3$. He has mentioned 400 nm emission in samples containing very small concentrations of Sn^{2+}. Apparently, only small quantities of Sn^{2+} are incorporated by the precipitation method.

In contrast to ns^2 activators, studies on rare earth activators in $CaSiO_3$ are few. Recently, Zhou and Yan [43] reported luminescence of Eu^{3+} in monoclinic beta-$CaSiO_3$ (parawollastonite) prepared by sol–gel method. They observed prominent f–f excitation and both the red and orange emission bands. We have also obtained similar results for triclinic beta $CaSiO_3$:Eu^{3+} prepared by the precipitation method. (Fig. 4, curves a and b). The emission spectrum consists of typical lines around 613 and 592 nm corresponding to $^5D_0$–$^7F_1$, $^7F_2$ transitions. The excitation spectrum consists of several sharp lines around 392, 382, 364, 324 and 304 nm corresponding to transitions $^7F_0 \rightarrow {}^5L_6$, $^7F_0 \rightarrow {}^5G$, $^7F_0 \rightarrow {}^5D_4$, $^7F_0 \rightarrow {}^5H$, $^7F_0 \rightarrow {}^5F$, respectively. The band around 250 nm can be attributed to charge transfer excitation. This is consistent with the results of the optical absorption studies reported by Zhou and Yan [43].

3.2. $SrSiO_3$

As precipitated powder of $SrSiO_3$ was poorly crystallized and no sharp line pattern was observed. The samples annealed at 700 °C for 1 h showed good crystallinity. Fig. 5 shows stick patterns deduced from the diffraction data obtained for the annealed $SrSiO_3$ samples. The patterns are compared with the major lines in the ICDD data file 36-0018 corresponding to monoclinic alpha-$SrSiO_3$. $SrSiO_3$ is thus formed at annealing temperature as low as 700 °C by the procedure described here.

Fig. 6 shows PL results for some ns^2 activators in $SrSiO_3$. A strong emission band is observed around 337 nm for Bi^{3+} (0.2 mol%) for 287 nm excitation (Fig. 6a and b). A broad shoulder is observed to this band at about 375 nm. The shoulder may be due to aggregation of the activator into pairs. Two emission bands were more distinctly observed for Pb^{2+}. The short wavelength emission band at 283 nm has a narrow excitation around 239 nm (Fig. 6c and d). A more complicated structure at longer wavelengths with a maximum around 367 nm is observed for 257 nm excitation. The longer wavelength emission bands may result from the activator in higher aggregation states. Klasens et al. [42] have mentioned weak Pb^{2+} emission in $SrSiO_3$.

Fig. 7 shows PL results for some rare earth activators in $SrSiO_3$. Ce^{3+} emission (Fig. 7, curve a) is in the violet range with a maximum around 410 nm. The corresponding excitation spectrum (Fig. 7, curve b) shows a prominent band around 327 nm with a shoulder at 349 nm. There is also a weak excitation around 280 nm.

PL spectra of Ce^{3+} can be conveniently discussed in terms of the scheme used by Dorenbos [44–46]. The Ce^{3+} ion has, from a spectroscopic point of view, a very simple electron configuration in the ground and excited state: $4f^1$ and $5d^1$, respectively. The $4f^1$ state is split by spin-orbit coupling into a doublet ($^2F_{5/2}$, $^2F_{7/2}$) with an energy difference of 2000 cm^{-1}. The $5d^1$ state is split by the crystal field into several components with an averaged total splitting of some 10,000 cm^{-1}. The emission consists of a transition from the lowest crystal-field component of the $5d^1$ state to the ground state. The emission band has two maxima due to the spin–orbit splitting of the ground state. The spin–orbit split $^2D_{3/2}$ and $^2D_{5/2}$ states of the 5d configuration of free Ce^{3+} are located at 49,700 and 52,100 cm^{-1} above the $4f^1$ ($^2F_{5/2}$) ground state of Ce^{3+}. When Ce^{3+} is introduced in a compound the average energy of the 5d configura-

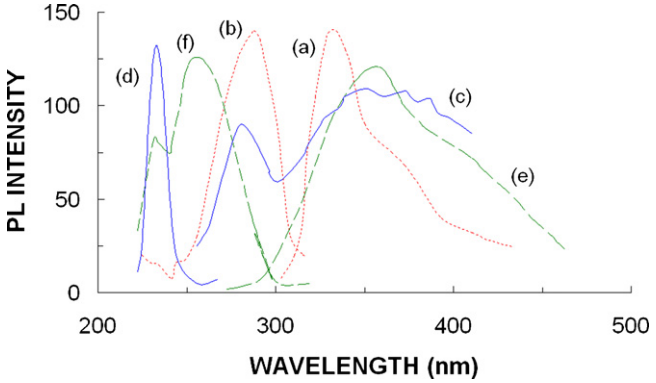

Fig. 6. Photoluminescence (PL) spectra of ns^2 activators in $SrSiO_3$. (a) Bi^{3+} emission for 290 nm excitation; (b) Bi^{3+} excitation for 337 nm emission; (c) Pb^{2+} emission for 239 nm excitation; (d) Pb^{2+} excitation for 290 nm emission; (e) Pb^{2+} emission for 257 nm excitation; (f) Pb^{2+} excitation for 367 nm emission.

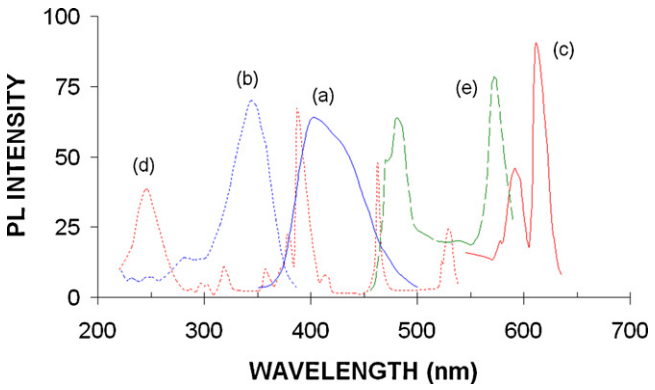

Fig. 7. Photoluminescence (PL) spectra of rare earth activators in $SrSiO_3$. (a) Ce^{3+} emission for 330 nm excitation; (b) Ce^{3+} excitation for 412 nm emission; (c) Eu^{3+} emission for 239 nm excitation; (d) Eu^{3+} excitation for 290 nm emission; (e) Dy^{3+} emission for 350 nm excitation.

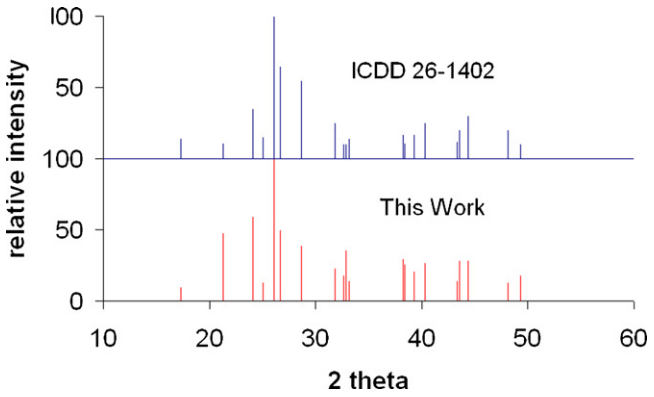

Fig. 8. XRD pattern for $BaSiO_3$. Stick pattern deduced from XRD data recorded for $BaSiO_3$ are compared with the major lines in the ICDD data file 26-1402 corresponding to orthorhombic beta-$BaSiO_3$. An excellent match is seen.

tion is lowered and the $^2D_{3/2}$ and $^2D_{5/2}$ states are further split by the crystal field. Depending on the site symmetry, at most five distinct 5d states may form. The energy difference between the maxima of the highest and lowest 5d bands in spectra is defined as the total crystal field splitting (cfs). The energy shift of the average of the 5d configuration is defined as the centroid shift (c). The combination of c and cfs leads to the redshift D defined as

$$D = 49,340 - 10^7/\lambda_1 \quad \mathrm{cm}^{-1}$$

where λ_1 is the wavelength (nm) of the first 5d absorption band in Ce^{3+}.

The energy of Ce^{3+} 5d → 4f emission in compound is given by, $E_{em} = E_{free} - D(A) - DS(A)$, where E_{free} is the lowest 4f → 5d Ce^{3+} transition energy in a free ion. $D(A)$ and DS(A) are the red shift and the Stokes shift, respectively. The red shift expresses the amount by which the energy of the first dipole-allowed 4f → 5d transition is lowered whenever the Ce^{3+} ion is doped in a host crystal. After 4f → 5d excitation, the level is further lowered by the Stokes shift due to lattice relaxation.

For $SrSiO_3$:Ce^{3+} the red shift is 20,686 cm^{-1} and the Stokes shift 4381 cm^{-1}. The doublet structure in the emission spectrum is barely observable, but the doublet splitting cannot be calculated from the spectrum as it is not resolved.

PL spectra for $SrSiO_3$:Eu^{3+} are also shown in Fig. 7 (curves c and d). f–f transitions of Eu^{3+} are forbidden and Eu^{3+} PL is in general weak, unless there is excitation by charge transfer or energy transfer from a sensitizer. In general, narrow emission bands may be observed at about 570, 590, 610, 650 and 700 nm corresponding to transitions $^5D_0 \rightarrow {}^7F_0$, $^7F_1$, $^7F_2$, $^7F_3$, $^7F_4$, respectively. Eu^{3+} emission usually occurs from $^5D_0 \rightarrow {}^7F_j$ transitions. There are three transitions which are of prime importance $^5D_0 \rightarrow {}^7F_0$ (around 570 nm), $^5D_0 \rightarrow {}^7F_1$ (around 595 nm) and $^5D_0 \rightarrow {}^7F_2$ (around 610 nm). The first one is strongly forbidden transition and yet observed with appreciable intensity in some hosts. $^5D_0 \rightarrow F_1$ transition is forbidden as electric dipole, but allowed as magnetic dipole. This is the only transition when Eu^{3+} occupies a site coinciding with a centre of symmetry. When Eu^{3+} ion is situated at a site, which lacks the inversion symmetry, then the transitions corresponding to even values of j (except 0) are electric dipole allowed and red emission can be observed. $^5D_0 \rightarrow {}^7F_1$ transition can also be observed as magnetic dipole allowed transition. Further, all the lines corresponding to these transitions split into number of components decided by the local symmetry.

For $SrSiO_3$:Eu^{3+}, emission lines are observed around 591 and 611 nm corresponding to $^5D_0 \rightarrow {}^7F_1$ and $^5D_0 \rightarrow {}^7F_2$ transitions, respectively. The excitation spectrum consists of a broad band around 250 nm which can be ascribed to charge transfer and several sharp lines attributable to f–f transitions. The f–f excitation lines can be seen at 530 nm ($^7F_0 \rightarrow {}^5D_1$), 470 nm ($^7F_0 \rightarrow {}^5D_2$), 410 nm ($^7F_0 \rightarrow {}^5D_3$), 395 nm ($^7F_0 \rightarrow {}^5L_6$), 380 nm ($^7F_0 \rightarrow {}^5G$), 365 nm ($^7F_0 \rightarrow {}^5D_4$), 325 nm ($^7F_0 \rightarrow {}^5H$) and around 300 nm ($^7F_0 \rightarrow {}^5F$).

Weak f–f emission was observed for $SrSiO_3$:Dy^{3+} also (Fig. 7, curve e) upon 350 nm excitation. Lines around 481 nm and 573 nm can be assigned to $^4F_{9/2} \rightarrow {}^6H_{15/2}$ and $^4F_{9/2} \rightarrow {}^6H_{15/2}$ transitions of Dy^{3+}, respectively. These results are similar to those reported by Kuang et al. [47] who studied $SrSiO_3$:Dy^{3+} as a long afterglow phosphor.

3.3. $BaSiO_3$

As precipitated powder of $BaSiO_3$ was poorly crystallized and no sharp line pattern was observed. The samples annealed at 700 °C for 1 h showed good crystallinity. Fig. 8 shows stick patterns deduced from the diffraction data obtained for the annealed $BaSiO_3$ samples. The patterns are compared with the major lines in the ICDD data file ICDD 26-1402 corresponding to orthorhombic beta-$BaSiO_3$. $BaSiO_3$ is thus formed at annealing temperature as low as 700 °C by the procedure described here. By the conventional solid state reaction technique, beta-$BaSiO_3$ is obtained only above 1100 °C.

Fig. 9 shows PL results for some ns^2 activators in $BaSiO_3$ host. Both Bi^{3+} and Pb^{2+} exhibited appreciable luminescence in $BaSiO_3$. Bi^{3+} emission excited by 280 nm is in the violet region, peaking at 400 nm (Fig. 9, curves a and b), while Pb^{2+} emission is in the UV region. The prominent peak is around 324 nm. There is also another

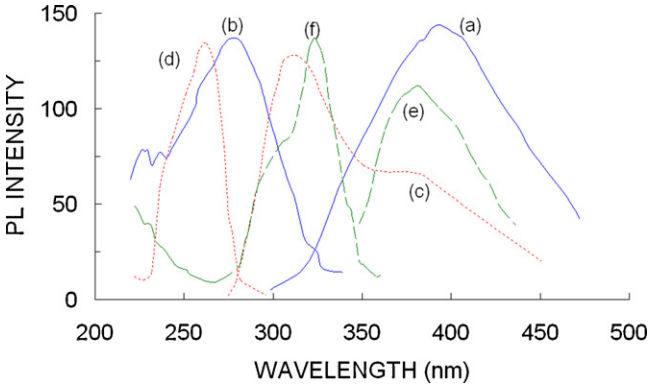

Fig. 9. Photoluminescence (PL) spectra of ns^2 and Ce^{3+} activators in $BaSiO_3$. (a) Bi^{3+} emission for 280 nm excitation; (b) Bi^{3+} excitation for 400 nm emission; (c) Pb^{2+} emission for 270 nm excitation; (d) Pb^{2+} excitation for 324 nm emission; (e) Ce^{3+} emission for 327 nm excitation; (f) Ce^{3+} excitation for 390 nm emission.

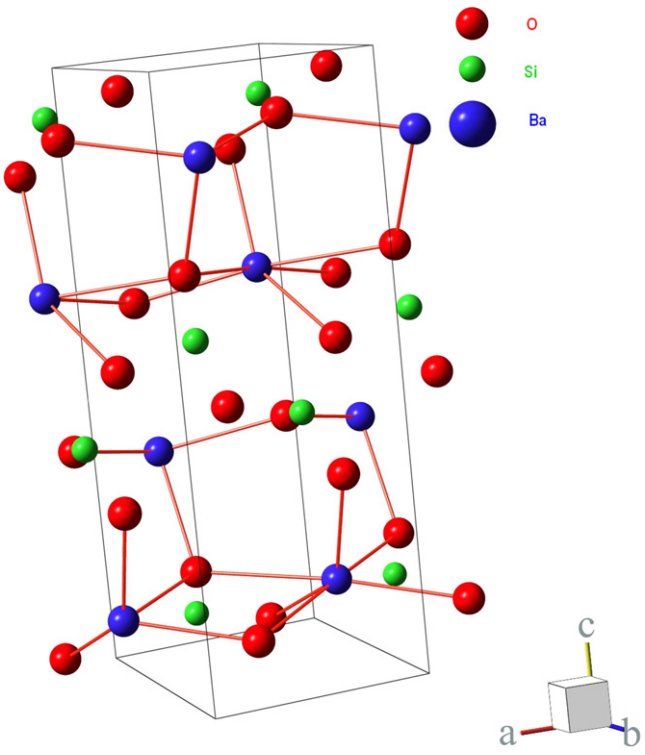

Fig. 10. Co-ordination of Pb^{2+} in beta $BaSiO_3$. Pb^{2+} is expected to be at Ba substitutional site and will have same co-ordination as Ba^{2+}.

band on the long wavelength side at about 375 nm which may be due to Pb^{2+} pairs. The excitation spectrum also shows structure with the prominent peak around 270 nm (Fig. 9, curves c and d). Pb^{2+} is expected to be present at Ba substitutional site coordinating with 6 oxygen ions (Fig. 10). Ce^{3+} emission is also in the violet/near UV region, in form of a broad band around 390 nm (Fig. 9, curve e). The excitation spectrum consists of a maximum around 327 nm with several shoulders around 290, 315 and 340 nm. These are characteristic of splitting of Ce^{3+} 5d levels in crystal field (Fig. 9, curve f). The results are in good agreement with those reported by Kelsey and Brown [48].

3.4. $MgSiO_3$

As precipitated powder of $MgSiO_3$ was poorly crystallized and no sharp line pattern was observed. The samples annealed at 700 °C for 1 h showed good crystallinity. The pattern matched with ICDD 76-0490.

Studies on luminescence in $MgSiO_3$ are few. There are no old data. In relatively recent times, thermoluminescence [49–51] which is important for study of meteors, photoluminescence of $3d^n$ activators like Mn^{2+} [52], Ni^{2+} and Cr^{3+} [53,54], which is important in context of eye-safe lasers, rare earth activators [55] like Dy^{3+} [56], Eu^{3+} [57], Eu^{2+} [34], etc. and long lasting phosphorescence of various activators [58] have been reported. There are no reports on luminescence of ns^2 activators in this host.

Results on PL in $MgSiO_3$ are more or less similar to those described for $BaSiO_3$. PL was observed for the ns^2 activators Bi^{3+} and Pb^{2+} and the rare earth Ce^{3+}. Bi^{3+} emission is around 345 nm. There is also another band on the long wavelength side at about 400 nm which may be due to Bi^{3+} pairs. The excitation spectrum also shows double humped, prominent peak with maxima at about 280 and 295 nm (Fig. 11, curves a and b). A shoulder can also be seen on the short wavelength side around 260 nm. Pb^{2+} PL exhibits much higher Stokes shift. The excitation maximum is around 265 nm while a

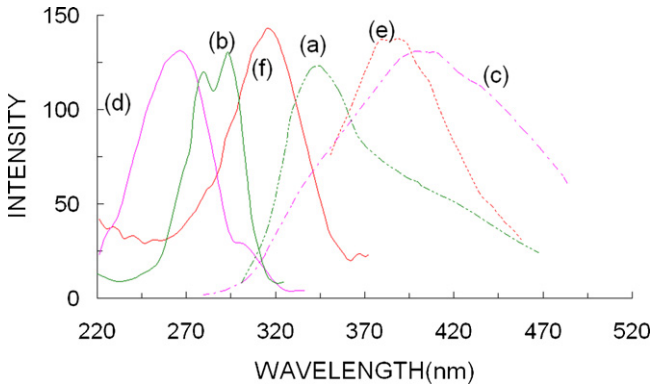

Fig. 11. Photoluminescence (PL) spectra of ns^2 and Ce^{3+} activators in $MgSiO_3$. (a) Bi^{3+} emission for 295 nm excitation; (b) Bi^{3+} excitation for 345 nm emission; (c) Pb^{2+} emission for 265 nm excitation; (d) Pb^{2+} excitation for 400 nm emission; (e) Ce^{3+} emission for 318 nm excitation; (f) Ce^{3+} excitation for 388 nm emission.

very broad emission is centred at 400 nm (Fig. 11, curves c and d). Ce^{3+} emission in the near UV region is also very broad. The excitation spectrum is better defined, exhibiting a prominent maximum around 318 nm with several shoulders around 282, 295 and 305 nm (Fig. 11, curves e and f). These are characteristic of splitting of Ce^{3+} 5d levels in crystal field.

4. Conclusions

Phase pure, alkaline earth metasilicates could be prepared by a new method based on precipitation followed by thermal annealing at 700 °C. This procedure is much simpler compared to the conventional solid state reactions involving heating at temperatures exceeding 1100 °C. Activation by various ns^2 dopants like Bi^{3+}, Sn^{2+} and Pb^{2+}, as well as the rare earth Ce^{3+}, Eu^{3+} and Dy^{3+} could also be achieved. Characteristic emissions which are in accordance with the literature results have been observed. Results on new phosphors $CaSiO_3$:Bi, $MgSiO_3$:Bi and $MgSiO_3$:Pb are reported. UV emission was observed for these phosphors. This method will prove useful for synthesis of metasilicates required for various applications.

References

[1] K. Byrappa, D. Yu, Pushcharovsky Prog. Cryst. Growth Charact. 24 (1992) 269.
[2] D. Yu, Pushcharovsky, Structural Mineralogy of Silicates and their Analogues, Nedra, Moscow, 1986, p.160 (in Russian).
[3] F. Ciesielczyk, A. Krysztafkiewicz, T. Jesionowski, J. Mater. Sci. 42 (2007) 3831.
[4] P. Jenkins, J. Ralston, Colloids Surf. A 139 (1998) 27.
[5] P. Huang, D.W. Fuerstenau, Colloids Surf. A 177 (2001) 147.
[6] M. Teixeira, C. Cavalheiro, L. Ramos, E.A. Neves, Appl. Clay Sci. 23 (2003) 323.
[7] C. Shu, X. Mingxia, Z. Cailou, T. Jiaqi, Mater. Res. Bull. 37 (2002) 1333.
[8] E. Kalinkina, A. Kalinkin, W. Forsling, V. Makarov, Int. J. Miner. Proc. 61 (2001) 289.
[9] A. Gladysz-Plaska, M. Majdan, M. Kowalska-Ternes, Przem. Chem. 82 (2003) 1435.
[10] K. Okada, M. Tanuma, Y. Kameshima, A. Nakajima, S. Asai, M. Sumita, Mater. Res. Bull. 44 (2009) 298.
[11] N. Zhang, J.A. Molenda, J.H. Fournelle, W.L. Murphy, N. Sahai, Biomaterials 31 (2010) 7653.
[12] N.-H. Nguyen, J.-B. Lim, S. Nahm, J.-H. Paik, J.-H. Kim, J. Am. Ceram. Soc. 90 (2007) 3127.
[13] D. Zhang, J. Chang, Mater. Chem. Phys. 118 (2009) 379.
[14] H.Y. Li, J. Chang, Biomaterials 25 (2004) 5473.
[15] H.Y. Li, J. Chang, J. Mater. Sci. Mater. Med. 15 (2004) 1.
[16] B.V. Zhmud, W.A. House, E.B. Sevastyanova, Colloids Surf. A 127 (1997) 187.
[17] T. Yamanaka, H. Mori, Acta Crystallogr. B37 (1981) 1010.
[18] A.J. Salinas, M. Vallet-Regi, I. Izquierdo-Barba, J. Sol-Gel Sci. Technol. 21 (2001) 13.
[19] X.Y. Liu, C.X. Ding, Biomaterials 23 (2002) 4065.
[20] X.H. Wan, C.K. Chang, D.L. Mao, L. Jiang, M. Li, Mater. Sci. Eng. C 25 (2005) 455.
[21] X.-H. Huang, J. Chang, Mater. Chem. Phys. 115 (2009) 1.
[22] T. Kokubo, S. Ito, Z. Huang, T. Hayashi, S. Sakka, T. Kitsugi, J. Biomed. Mater. Res. 24 (1990) 331.

[23] M.K. Galperina, N.S. Lykhina, Glass Ceram. 33 (1976) 172.
[24] A. Mali, A. Ataie, J. Alloys Compd. 399 (2005) 245.
[25] R.W. Mooney, J. Electrochem. Soc. 106 (1959) 955.
[26] Y. Shimizu, Y. Syono, S. Akimoto, High Temp. High Press. 2 (1970) 113.
[27] K.-I. Machida, G.-Y. Adachi, J. Shiokawa, M. Shimada, M. Koizumi, Acta Crystallogr. B38 (1982) 386.
[28] O.B. Tagiev, S.A. Abushov, F.A. Kazymova, K.O. Tagiev, J. Appl. Spectrosc. 73 (2006) 541.
[29] A.N. Georgobiani, C. Barthou, P. Benalloul, I.B. Bakhtiyarly, K.O. Tagiev, Inorg. Mater. 45 (2009) 1032.
[30] H.C. Frolich, J. Electrochem. Soc. 93 (1948) 101.
[31] J. Yang, L. Yang, W. Liu, Y. Zhang, H. Fan, Y. Wang, H. Liu, J. Lang, D. Wang, J. Alloys Compd. 454 (2008) 506.
[32] H. Liu, Y. Wang, J. Yang, L. Li, W. Su, Z. Guan, B. Yu, J. Alloys Compd. 191 (1993) 1.
[33] Z. Cui, R. Ye, D. Deng, Y. Hua, S. Zhao, G. Jia, C. Li, S. Xu, J. Alloys Compd. 509 (2011) 3553.
[34] L. Lin, C. Shi, Z. Wang, W. Zhang, M. Yin, J. Alloys Compd. 466 (2008) 546.
[35] S. Chen, X. Zhou, S. Zhang, B. Li, T. Zhang, J. Alloys Compd. 505 (2010) 613.
[36] T. Tang, Z. Zhang, J.-B. Meng, D.-L. Luo, Fusion Eng. Des. 84 (2009) 2124.
[37] Y.P. Naik, M. Mohapatra, N.D. Dahale, T.K. Seshagiri, V. Natarajan, S.V. Godbole, J. Lumin. 129 (2009) 1225.
[38] I. Halasz, M. Agarwal, R. Li, N. Miller, Micropor. Mesopor. Mater. 135 (2010) 74.
[39] F. Agullo-Lopez, J.M. Calleja, F. Cuso, F. Jaque, F.J. Lopez, Prog. Mater. Sci. 30 (1986) 187.
[40] G. Blasse, Prog. Solid State Chem. 18 (1988) 79.
[41] A. Ranfagni, D. Mugnai, M. Bacci, G. Viliani, M.P. Fontana, Adv. Phys. 32 (1983) 823.
[42] H.A. Klasens, A.H. Hoekstra, A.P.M. Cox, J. Electrochem. Soc. 104 (1957) 93.
[43] L. Zhou, B. Yan, J. Phys. Chem. Solids 69 (2008) 2877.
[44] P. Dorenbos, J. Lumin. 91 (2000) 155.
[45] P. Dorenbos, J. Lumin. 91 (2000) 91.
[46] P. Dorenbos, Phys. Rev. B65 (2002) 235110.
[47] J. Kuang, Y. Liu, J. Zhang, J. Solid State Chem. 179 (2006) 266.
[48] P.V. Kelsey Jr., J.J. Brown Jr., J. Electrochem. Soc. 123 (1976) 1384.
[49] H. Nagabhushana, B.M. Nagabhushana, B. Umesh, H.B. Premkumar, N. Anil, T.K. Gundu Rao, R.P.S. Chakradhar, Philos. Mag. 90 (2010) 1567.
[50] K. Koike, M. Nakagawa, C. Koike, M. Okada, H. Chihara, Astron. Astrophys. 390 (2002) 1133.
[51] R.T. Greer, Mater. Res. Bull. 5 (1970) 765.
[52] L. Lin, M. Yin, C. Shi, W. Zhang, B. You, J. Rare Earths 24 (2006) 104.
[53] R. Moncorge, M. Bettinelli, Y. Guyot, E. Cavalli, J.A. Capobianco, S. Girard, J. Phys. Condensed Matter 11 (1999) 6831.
[54] E. Cavalli, M. Bettinelli, Opt. Mater. 2 (1993) 151.
[55] X. Fan, M. Wang, Z. Wang, Mater. Sci. Eng. B 47 (1997) 252.
[56] S. Wang, X. Xie, H. Wu, Y. Shi, C. Zhuang, X. Chem, J. Tsinghua Univ. 50 (2010) 896.
[57] X. Fan, M. Wang, Y. Yu, Q. Wu, J. Phys. Chem. Solids 57 (1996) 1259.
[58] X.J. Wang, D. Jia, W.M. Yen, J. Lumin. 102–103 (2003) 34.